Kinetics and Mechanism of Forsterite Dissolution at 25°C and pH from 1 to 12

Article *in* Geochimica et Cosmochimica Acta · October 2000

Impact Factor: 4.33 · DOI: 10.1016/S0016-7037(00)00434-8

2 authors:

Oleg S. Pokrovsky
GET UMR 5563 CNRS, IEPS RAS Arkhangels…
264 PUBLICATIONS **5,346** CITATIONS
SEE PROFILE

Jacques Schott
French National Centre for Scientific Resea…
255 PUBLICATIONS **10,072** CITATIONS
SEE PROFILE

Pergamon

Geochimica et Cosmochimica Acta, Vol. 64, No. 19, pp. 3313–3325, 2000

0016-7037/00 $20.00 + .00

PII S0016-7037(00)00434-8

Kinetics and mechanism of forsterite dissolution at 25°C and pH from 1 to 12

OLEG S. POKROVSKY* and JACQUES SCHOTT

Géochimie: Transferts et Mécanismes, CNRS (UMR 5563)-OMP-Université Paul-Sabatier, 38 rue des Trente-Six Ponts, 31400 Toulouse, France

(*Received November* 5, 1999; *accepted in revised form April* 18, 2000)

Abstract—The forward dissolution rate of San Carlos forsterite Fo_{91} was measured at 25°C in a mixed-flow reactor as a function of pH (1 to 12), ionic strength (0.001 to 0.1 M), ΣCO_2 (0 to 0.05 M), aqueous magnesium (10^{-6} to 0.05 M) and silica (10^{-6} to 0.001 M) concentrations. In CO_2-free solutions, the rates decrease with increasing pH at $1 \leq pH \leq 8$ with a slope close to 0.5. At $9 \leq pH \leq 12$, the rates continue to decrease but with a smaller slope of ~0.1. Addition of silica to solution at pH above 8.8 leads to reduction of up to 5 times in the dissolution rate. Magnesium ions have no effect on forsterite dissolution rate at pH from 3 to 6 and $10^{-5} < [Mg^{2+}]_{tot} < 0.04$ M. Aqueous carbonate ions strongly inhibit dissolution in alkaline solutions when $aCO_3^{2-} > 10^{-4}$ M. In acidic and slightly alkaline solutions, forsterite dissolution is controlled by the decomposition of a silica-rich/magnesium-deficient protonated precursor complex. This complex is formed by exchange of two hydrogen ions for a Mg atom on the forsterite surface followed by polymerization of partially protonated SiO_4 tetrahedra and rate-controlling H^+ penetration into the leached layer and its adsorption on silica dimers. This accounts for the observed 0.5 order dependence of dissolution rate on H^+ activity. In alkaline solutions, dissolution is controlled by the decomposition of Mg hydrated sites in a Mg-rich layer formed by silica preferential release. Within this conceptual model, forsterite forward rate of dissolution can be accurately described for a wide variety of solution compositions assuming two parallel reactions occurring at silica-rich and hydrated Mg surface sites:

$$R_+ \text{ (mol/cm}^2\text{/s)} = 2.38 \times 10^{-11} \{>Si_2O\text{-}H^+\} + 1.62 \times 10^{-10} \{>MgOH_2^+\}$$

where $\{>i\}$ stands for surface species concentration (mol/m^2). This equation describes the weak dependence of dissolution rates on pH in alkaline solutions and the inhibiting effect of carbonate ions and dissolved silica when the hydration of surface Mg atoms with formation of $>MgOH_2^+$ is the rate-controlling step for dissolution. It follows that the decrease of forsterite dissolution rate with increasing carbonate concentration at $pH \geq 9$ in natural aquatic systems results in a decrease of atmospheric CO_2 consumption, i.e., unlike for feldspars, there is a negative feedback between pCO_2 and forsterite weathering rate. This should be taken into account when modeling the effect of mafic mineral weathering on CO_2 global balance. *Copyright © 2000 Elsevier Science Ltd*

1. INTRODUCTION

In the first part of this work (Pokrovsky and Schott, 2000), an approach utilizing a range of spectroscopic and of chemical techniques has been taken for the first time to characterize the surface chemistry of forsterite in aqueous solution as a function of solution composition and pH. The purpose of the present study is to apply these results for modeling forsterite dissolution kinetics in aquatic systems. Numerous studies have been devoted to the dissolution kinetics of forsterite (Luce et al., 1972; Sanemasa et al., 1972; Grandstaff, 1978; Siever and Woodford, 1979; Eriksson, 1982; Sverdrup and Bjerle, 1982; Siegel and Pfannkuch, 1984; Schott and Berner, 1983, 1985; Grandstaff, 1986; Blum and Lasaga, 1988; Sverdrup, 1990; Wogelius and Walther, 1991; Wogelius and Walther, 1992; Westrich et al., 1993; Oelkers, 1999; Awad et al., 2000; Chen and Brantley, 2000; Oelkers, 2000; Rosso and Rimstidt, 2000). In these studies, it has been recognized that at 25°C and pH < 7 forsterite dissolves congruently and the rate is proportional to either a_{H^+} (Murphy and Helgeson, 1987; Sverdrup, 1990, and references therein) or to $a_{H^+}^{0.5}$ (Wogelius and Walther, 1991; Wogelius and Walther, 1992; Rosso and Rimstidt, 2000). In alkaline solutions, the rate was found to increase with pH with a slope close to 1/3, similar to that for quartz and feldspars (Blum and Lasaga, 1988; Wogelius and Walther, 1991) which allowed Brady and Walther (1989) to suggest that, as for quartz and aluminosilicates, the breaking of Si-O bonds controls forsterite dissolution. However, one may question the validity of this mechanism because the structure of forsterite consists of isolated silica tetrahedra linked together by magnesium octahedra so that no critical Si-O bond has to be broken in order to destroy the mineral structure (Schott and Berner, 1983, Casey et al., 1993; Oelkers, 2000). Moreover, such a dissolution mechanism is inconsistent with the strong inhibiting effect of dissolved CO_2 at pH above 9 reported by Wogelius and Walther (1991). The adsorption of carbonate ions can only occur on the positively charged Mg surface groups which thus have to participate in the control of forsterite dissolution. In order to resolve these controversies, a systematic study of forsterite dissolution kinetics has been conducted at 25°C over a wide variety of solution compositions. The results enable a better description of forsterite chemical weathering rates and its effect on atmospheric CO_2 mass balance.

*Author to whom correspondence should be addressed (oleg@lucid.ups-tlse.fr).

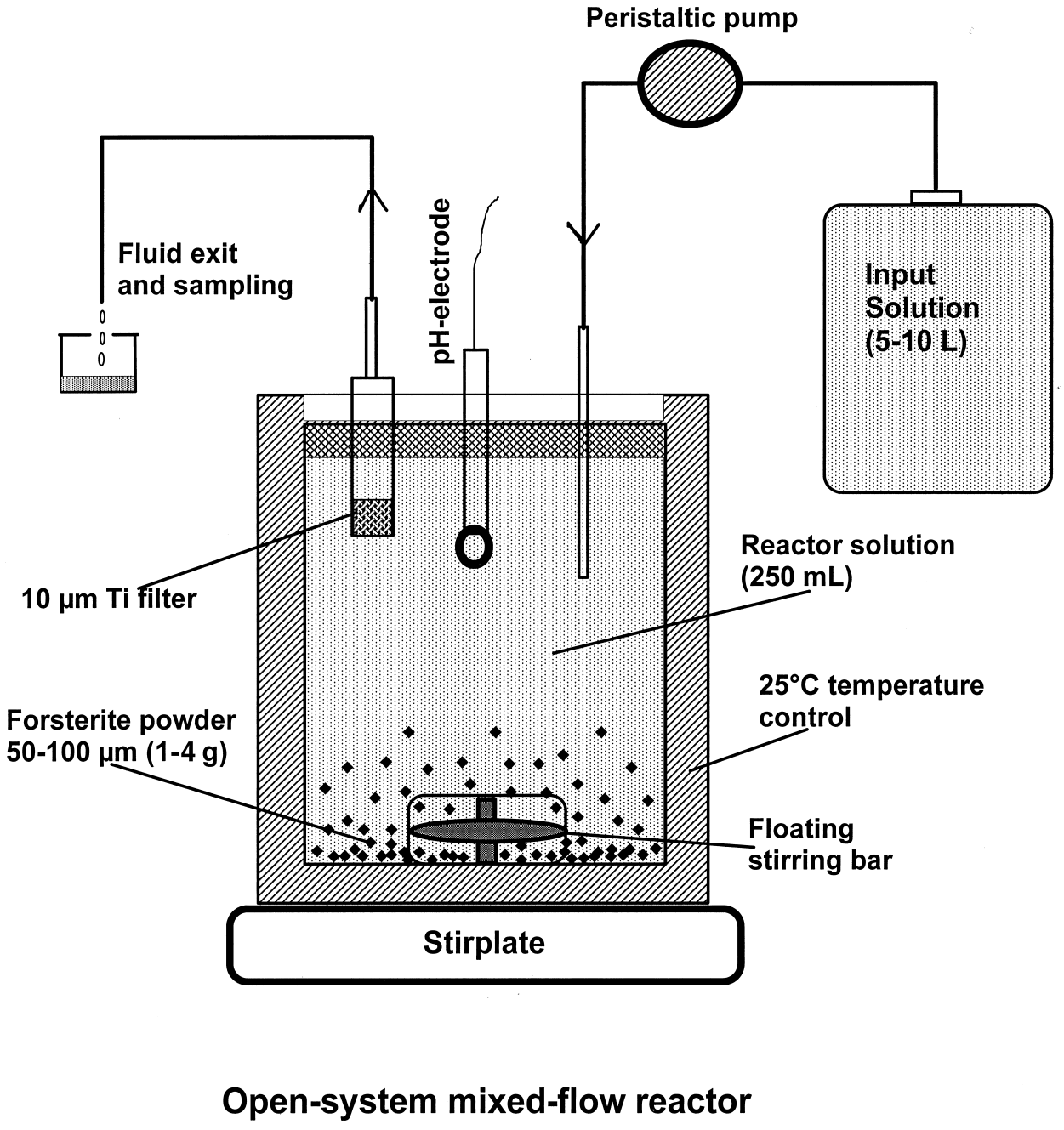

Fig. 1. Schematic setup of the mixed-flow reactor system.

2. MATERIALS AND METHODS

Forsterite from San Carlos (Arizona) was used in this study. The chemical analysis of this sample is given in Pokrovsky and Schott (2000) and corresponds to the composition $Mg_{1.82}Fe_{0.18}SiO_4$ (Fo_{91}). X-ray diffraction analysis of this material before and after experiments revealed neither contamination by clay minerals nor the formation of secondary phases. Transparent crystals ~0.5 cm in size were hand-picked, ground with an agate mortar and pestle, and sieved. The size fraction between 50 and 100 μm was ultrasonically cleaned using alcohol to remove fine particles and dried overnight at 60°C. The specific surface area of the cleaned powder was 800 $\pm$ 20 cm^2/g as determined by Kr adsorption using the multi-point B.E.T. method. Microscopic analysis of fresh and altered forsterite surfaces was performed using a Jeol JSM840a scanning electron microscope.

Steady-state dissolution rates were obtained at distinct solution compositions and pH using a mixed-flow reaction vessel immersed in a water bath held at a constant temperature of 25.0 $\pm$ 0.5°C. The experimental setup is depicted in Figure 1. The input fluid was stored in a compressible polyethylene container during the experiments. It was injected into the reaction vessel using a Gilson® peristaltic pump that allows flow rates ranging from 0.01 to 10 mL/min. The reactor consisted of a 250 mL Azlon® plastic beaker which was continuously stirred with a floating teflon supported magnetic stirrer. Stirring was controlled by a stirplate located directly beneath the bath. The reactive solution left the reactor through a 5 μm pore size Ti filter. Several

outlet solutions were additionally filtered through a 0.45 μm acetate filter. No differences in analytical Mg and Si concentrations were detected compared to 5 μm Ti filtered samples. A combined pH-electrode was inserted through the reactor cover to enable in-situ pH measurements for several experiments. The fluid composition can be regulated by either changing the flow rate or the composition of the inlet solution without dismantling the reactor and/or changing the amount of mineral present during the experiment. Between 1 and 4 g of forsterite was allowed to react in fluids of prescribed input compositions. Varying the mass of reacting forsterite from 0.5 to 4.0 g did not change the normalized dissolution rate.

Reacting fluids were comprised of deionized degassed H_2O, Merck reagent grade HCl, NaOH, $NaHCO_3$, Na_2CO_3, NaCl, and $MgCl_2$. In CO_2-free experiments, fresh input solution was purged of CO_2 by bubbling wet pure nitrogen for 10–12 h; this bubbling was repeated once every two days during long-term dissolution experiment. Regular control of alkalinity and pH in inlet solutions for CO_2-free experiments did not reveal any detectable dissolution of atmospheric CO_2 via diffusion through polyethylene walls of the container during the course of the experiments. Solution compositions used in the present study are listed in Tables 1 and 2.

All input and output solutions were analyzed for magnesium ($[Mg^{2+}]_{tot}$), silica ($[SiO_2(aq)]_{tot}$), alkalinity ([Alk]), and pH as a function of time. NBS buffers (pH = 4.008, 6.865, and 9.180 at 25°C) were used for calibration of a combination pH-electrode (Schott Geräte H62). Precision of pH measurement was $\pm$0.002 units. Alkalinity was determined following a standard HCl titration procedure with an uncertainty of $\pm$1% and a detection limit of 5×10^{-5} M. Magnesium and iron concentrations were measured by flame atomic absorption spectroscopy with an uncertainty of 1% and a detection limit of 1×10^{-7} and 3×10^{-7} M, respectively. Total silica concentration was determined using the molybdate blue method with an uncertainty of 2% and a detection limit of 3×10^{-7} M.

Homogeneous solution equilibria as well as surface speciation were calculated for each solution composition using the MINTEQA2 code and MINTEQA2 thermodynamic database (Allison et al., 1991). The activity coefficients of free ions and charged complexes were calculated using the Davies equation which is standard in MINTEQA2.

3. RESULTS AND DISCUSSION

Results of 101 steady-state dissolution experiments performed in CO_2-free and CO_2-bearing solutions at pH from 1 to 12 and ionic strength from 0.001 to 0.1 M are listed in Tables 1 and 2, respectively. The data are sorted by decreasing dissolution rate. Included in this table are reacting solid surface area, fluid flow rates, inlet fluid composition (or blank concentrations), outlet fluid pH, [Alk], $[Mg^{2+}]_{tot}$, $[SiO_2(aq)]_{tot}$, and steady-state forsterite dissolution rates.

Steady-state dissolution rates (R_i, mol/cm^2/s) given in Table 2 were computed from measured solution composition using

$$R_{Si} = -q \cdot \Delta[SiO_2(aq)]_{tot}/s$$

and

$$R_{Mg} = -q \cdot 0.56 \cdot \Delta[Mg^{2+}]_{tot}/s$$

where q (L/s) designates the fluid flow rate, $\Delta[SiO_2(aq)]_{tot}$ and $\Delta[Mg^{2+}]_{tot}$ (mol/L) stands for the difference between the input and output silica and magnesium solution concentration, respectively, and s (cm^2) refers to the total mineral surface area. The surface area used to calculate the rates listed in Tables 1 and 2 was that measured on the fresh (unreacted) forsterite powder.

Uncertainties on the steady-state rate constants given in Tables 1 and 2 are 10–15% and are dominated by the uncertainty on BET surface area measurements ($\pm$10%) and the standard deviation on average Mg or Si concentration at steady-state ($\pm$2% and $\pm$10% in acid and alkaline solutions, respectively). Repeated dissolution runs performed in solutions of similar composition on the same mineral powder indicate that dissolution rates do not vary by more than ~10% after elapsed times of greater than 150 h. Moreover, forsterite specific surface area decreased by less than 10% during dissolution experiments lasting more than 200 h as confirmed by B.E.T. surface area measurements. The lowest measurable rates were about 10^{-16} mol/cm^2/s which originated from the analytical detection limits and lowest Mg and Si concentration in blank experiments.

Steady state was typically reached after 6 to 100 h depending on the flow rate. For each experiment, at least 5 data points at steady-state conditions were collected. An example of steady state attainment at pH ~ 3 is shown in Figure 2 where outlet Mg and Si concentrations are plotted as a function of time. It can be seen that within the uncertainties of measurements ($\pm$10%), outlet Mg and Si concentrations remain constant during the course of the 10–30 h experiments. This demonstrates that the times necessary to reach mechanical (~four fluid residence times) and chemical steady-states are very close. In alkaline solutions, the time to reach the stoichiometric steady-state dissolution at the same flow rate was much longer, up to 200–300 h.

For all experiments listed in Tables 1 and 2, the outlet solutions were strongly undersaturated with respect to forsterite, brucite, and magnesite (saturation indices are below 0.02). For some experiments performed in alkaline solutions (i.e., Nos. 4, 5, 6, 17, 19), supersaturation with respect to chrysotile and talc was found. However, the stoichiometric release of Mg relative to Si at steady-state conditions suggests that precipitation of these silicate phases did not occur within the duration of experiments. Moreover, experiments 19-2 and 19-3 (Table 1) with solution saturation indices with respect to chrysotile of 0.2 and 12, respectively, exhibited very close values of R_{Mg}, thus demonstrating the absence of secondary phase precipitation. X-ray diffraction analysis of the grains reacted in alkaline solutions did not reveal any changes in mineralogical composition.

SEM examination of the surface of reacted grains showed that they are similar to those of the fresh powder (Fig. 3a). For acid-reacted grains, formation of etch pits can be clearly detected (Fig. 3b). For grains reacted in alkaline solutions, no alteration of the surface has been observed (Fig. 3c) thus confirming the absence of any secondary precipitation. This is in agreement with SEM analyses of Wogelius and Walther (1991) who did not detect the precipitation of any secondary silicate minerals in solutions about a hundred times supersaturated with respect to talc and/or chrysotile.

3.1. Dissolution Rates as a Function of Solution Composition

Forsterite steady-state dissolution rates measured at 25°C in CO_2-free solutions at ionic strengths ranging from 0.001 to 0.1 M are depicted as a function of pH in Figure 4. For comparison, Fo_{91} dissolution rates determined by Wogelius and Walther (1991) at low ionic strength (I $<$ 0.001 M, H_2O/HCl/NaOH) are shown in the same figure. There is a general agreement between Wogelius and Walther's (1991) rates and those obtained in the present study at pH from 2 to 8. The small differences at low pH values may be associated with the influence of ionic strength whereas the differences in alkaline solutions may be due to the fact that the dissolution rates reported

Table 1. Summary of Fo_{91} dissolution experiments performed at 25°C in CO_2-free solutions. The units of R are mol/cm^2/s. Background electrolyte is NaCl. pH is adjusted by HCl/NaOH addition. N.D. = not determined.

Exp #	Duration hrs.	Surface area, cm^2	Flow rate, mL/min	Ionic strength, M	pH	[Alk], M	[Mg^{2+}], M input	[Mg^{2+}], M output	[ΣSi], M input	[ΣSi], M output	$-\log R_{Si}$	$-\log R_{Mg}$
28–1	8	3072	3.17	0.1	1.03	N.D.	0	6.45×10^{-4}	0	3.4×10^{-4}	11.23	11.21
28–2	20	3008	1.27	0.1	1.12	N.D.	0	1.31×10^{-3}	0	7.30×10^{-4}	11.28	11.28
28–3	26	2880	0.633	0.1	1.11	N.D.	0	2.38×10^{-3}	0	1.23×10^{-3}	11.33	11.30
27–1	8	3200	3.12	0.1	2.13	N.D.	0	2.49×10^{-4}	0	1.24×10^{-4}	11.70	11.65
27–2	16	3200	1.67	0.1	2.18	N.D.	0	4.30×10^{-4}	0	2.26×10^{-4}	11.71	11.68
27–3	28	3200	0.644	0.1	2.21	N.D.	0	1.07×10^{-3}	0	5.71×10^{-4}	11.72	11.70
13–1	39	800	0.802	0.1	2.70	N.D.	0	2.02×10^{-4}	0	1.12×10^{-4}	11.73	
13–2	42	800	0.586	0.1	2.81	N.D.	0	2.21×10^{-4}	0	1.24×10^{-4}	11.82	
13–3	70	800	0.391	0.1	2.82	N.D.	0	2.97×10^{-4}	0	1.65×10^{-4}	11.89	
13–4	30	800	0.580	0.1	2.74	N.D.	0	2.32×10^{-4}	0	1.28×10^{-4}	11.83	
13–5	26	800	0.552	0.1	2.88	N.D.	0.00722	0.00725	0	1.14×10^{-4}	11.90	
13–6	48	800	0.552	0.1	2.89	N.D.	0.0130	0.0130	0	9.40×10^{-5}	11.96	
24–1	31	800	1.46	0.1	2.99	N.D.	0	7.45×10^{-5}	0	3.90×10^{-5}	11.93	
24–2	36	800	0.918	0.1	3.03	N.D.	0	1.02×10^{-4}	0	6.18×10^{-5}	11.97	
12–1	25	800	0.903	0.1	3.08	N.D.	0	7.94×10^{-5}	0	4.02×10^{-5}	12.14	
12–2	48	800	0.658	0.1	3.05	N.D.	0	9.47×10^{-5}	0	4.98×10^{-5}	12.18	
12–3	66	800	0.423	0.1	3.16	N.D.	0	1.22×10^{-4}	0	6.56×10^{-5}	12.25	
12–4	75	800	0.207	0.1	3.26	N.D.	0	2.03×10^{-4}	0	1.12×10^{-4}	12.34	
12–5	51	800	0.407	0.1	3.05	N.D.	0	1.17×10^{-4}	0	6.57×10^{-5}	12.28	
23–1	26	1600	0.980	0.001	4.15	$<10^{-5}$	0	1.58×10^{-5}	0	9.20×10^{-6}	13.03	13.05
23–2	31	1600	0.970	0.001	3.60	$<10^{-5}$	0	2.85×10^{-5}	0	1.57×10^{-5}	12.80	12.80
23–3	26	1600	0.975	0.001	3.34	$<10^{-5}$	0	5.15×10^{-5}	0	2.75×10^{-5}	12.55	12.54
23–4	28	1600	0.970	0.001	2.85	$<10^{-5}$	0	9.23×10^{-5}	0	4.96×10^{-5}	12.30	12.29
14–1	35	800	0.746	0.1	4.20	$<10^{-5}$	0	2.64×10^{-5}	0	1.33×10^{-5}	12.69	
14–2	42	800	0.570	0.1	4.41	$<10-^{5}$	0	2.50×10^{-5}	0	1.35×10^{-5}	12.80	
14–3	70	800	0.387	0.1	4.49	$<10^{-5}$	0	2.60×10^{-5}	0	1.30×10^{-5}	12.98	
14–4	30	800	0.570	0.1	4.22	$<10^{-5}$	0	2.84×10^{-5}	0	1.40×10^{-5}	12.78	
15–1	42	800	0.769	0.1	4.77	$<10^{-5}$	0	1.11×10^{-5}	0	6.9×10^{-6}	12.98	
15–2	42	800	0.585	0.1	4.85	$<10^{-5}$	0	1.45×10^{-5}	0	8.3×10^{-6}	13.02	
15–3	70	800	0.399	0.1	4.95	$<10^{-5}$	0	1.61×10^{-5}	0	9.0×10^{-6}	13.15	
15–4	26	800	0.580	0.1	4.55	$<10^{-5}$	0	1.44×10^{-5}	0	8.3×10^{-6}	13.03	
11–1	25	800	0.929	0.1	5.70	$<10^{-5}$	0	3.38×10^{-6}	0	1.69×10^{-6}	13.49	13.44
11–2	48	800	0.680	0.1	6.18	$<10^{-5}$	0	3.24×10^{-6}	0	1.80×10^{-6}	13.60	13.60
11–3	66	800	0.430	0.1	6.28	$<10^{-5}$	0	3.83×10^{-6}	0	2.08×10^{-6}	13.72	13.73
11–4	75	800	0.213	0.1	6.13	$<10^{-5}$	0	5.58×10^{-6}	0	2.74×10^{-6}	13.92	13.86
11–5	51	800	0.419	0.1	5.61	$<10^{-5}$	0	3.48×10^{-6}	0	1.87×10^{-6}	13.79	13.77
8–2	138	800	0.193	0.1	7.33	$<10^{-5}$	0	5.65×10^{-6}	0	2.85×10^{-6}	13.93	13.90
8–3	270	800	0.075	0.1	7.19	$<10^{-5}$	0	9.20×10^{-6}	0	5.0×10^{-6}	14.11	14.10
8–4	111	800	0.184	0.1	7.21	$<10^{-5}$	0	4.15×10^{-6}	0	2.4×10^{-6}	14.04	14.05
8–5	96	800	0.370	0.1	7.25	$<10^{-5}$	0	2.95×10^{-6}	0	1.7×10^{-6}	13.88	13.90
25–1a	30	1600	0.631	0.1	6.60	$<10^{-5}$	0	N.D.	0	1.63×10^{-6}	13.97	N.D.
25–1b	56	1600	0.316	0.1	6.39	$<10^{-5}$	0	5.60×10^{-6}	0	2.78×10^{-6}	14.04	13.99
25–2	48	1600	0.315	0.1	6.37	$<10^{-5}$	1.38×10^{-4}	1.41×10^{-4}	0	2.98×10^{-6}	14.01	N.D.
25–3	48	1600	0.314	0.1	6.30	$<10^{-5}$	4.38×10^{-4}	4.40×10^{-4}	0	2.80×10^{-6}	14.04	N.D.
25–4	47	1600	0.315	0.1	6.29	$<10^{-5}$	7.55×10^{-4}	7.56×10^{-4}	0	2.69×10^{-6}	14.05	N.D.
25–5	45	1600	0.317	0.1	6.29	$<10^{-5}$	0.00118	0.00118	0	2.75×10^{-6}	14.04	N.D.
25–6	46	1600	0.316	0.1	6.28	$<10^{-5}$	0.00320	0.00320	0	2.50×10^{-6}	14.08	N.D.
25–7	48	1600	0.317	0.1	6.32	$<10^{-5}$	0.0450	0.0450	0	2.57×10^{-6}	14.07	N.D.
7–2	138	1600	0.395	0.1	9.30	1.0×10^{-4}	0	1.03×10^{-6}	0	7.9×10^{-7}	14.49	14.63
7–3	290	1600	0.0782	0.1	7.90	1.0×10^{-4}	0	6.36×10^{-6}	0	3.30×10^{-6}	14.57	14.59
7–4	112	1600	0.193	0.1	7.60	1.1×10^{-4}	0	3.19×10^{-6}	0	1.70×10^{-6}	14.47	14.45
7–5	45	1600	0.394	0.1	7.98	1.0×10^{-4}	0	1.60×10^{-6}	0	1.50×10^{-6}	14.39	14.44
1–2	91	1600	0.552	0.02	10.24	3.06×10^{-4}	0	6.0×10^{-7}	0	N.D.		14.72
1–3	88	1600	0.184	0.02	10.08	3.23×10^{-4}	0	1.35×10^{-6}	0	8.4×10^{-7}	14.79	14.89
1–4	126	1600	0.074	0.02	9.58	3.60×10^{-4}	0	2.40×10^{-6}	0	3.77×10^{-6}	14.54	15.03
4–3	300	1600	0.107	0.1	10.76	0.00108	0	3.85×10^{-6}	0	3.7×10^{-6}	14.38	14.62
4–4	112	1600	0.206	0.1	10.90	0.00107	0	2.22×10^{-6}	0	1.7×10^{-6}	14.44	14.58
5–3	230	1600	0.136	0.02	12.06	0.010	0	1.81×10^{-6}	0	1.0×10^{-6}	14.85	14.85
6–2	140	1600	0.197	0.1	10.90	0.00101	0	2.05×10^{-6}	0	1.0×10^{-6}	14.69	14.68
6–3	180	1600	0.0773	0.1	10.78	9.55×10^{-4}	0	2.83×10^{-6}	0	1.4×10^{-6}	14.95	14.94
18–2	120	800	0.240	0.1	11.45	0.00310	0	3.6×10^{-7}	3.5×10^{-7}	4.8×10^{-7}	15.19	15.01
18–3	162	800	0.126	0.1	11.42	0.00303	0	4.3×10^{-7}	3.5×10^{-7}	6.0×10^{-7}	15.18	15.20
18–4	290	800	0.0733	0.1	11.46	0.00305	0	N.D.	3.5×10^{-7}	7.2×10^{-7}	15.25	15.17
18–5	250	800	0.147	0.1	11.50	0.00305	0	6.2×10^{-7}	3.5×10^{-7}	6.6×10^{-7}	15.02	14.98

(Continued)

Table 1. (Continued)

Exp #	Duration hrs.	Surface area, cm^2	Flow rate, mL/min	Ionic strength, M	pH	[Alk], M	$[Mg^{2+}]$, M input	$[Mg^{2+}]$, M output	[ΣSi], M input	[ΣSi], M output	$-\log R_{Si}$	$-\log R_{Mg}$
19–2	106	1600	0.221	0.1	10.95	0.00150	0	8.05×10^{-7}	0	1.1×10^{-6}	14.60	14.99
19–3	135	1600	0.111	0.1	10.85	0.00152	0	1.50×10^{-6}	0	4.2×10^{-6}	14.31	15.02
19–4	123	1600	0.110	0.1	11.14	0.00151	0	6.7×10^{-7}	7.7×10^{-4}	7.7×10^{-4}	N.D.	15.37
20–2	106	1600	0.202	0.0015	11.01	0.00148	0	2.47×10^{-6}	0	1.27×10^{-6}	14.57	14.54
20–3	135	1600	0.099	0.0015	11.13	0.00151	0	3.13×10^{-6}	0	1.90×10^{-6}	14.71	14.75
20–4	123	1600	0.100	0.0015	11.26	0.00150	0	5.5×10^{-7}	8.0×10^{-4}	8.0×10^{-4}	N.D.	15.50
21–2	106	1600	0.213	0.001	8.02	$<10^{-4}$	0	6.09×10^{-6}	0	3.38×10^{-6}	14.13	14.13
21–3	135	1600	0.105	0.001	8.13	$<10^{-4}$	0	8.85×10^{-6}	0	4.30×10^{-6}	14.33	14.27
21–4	123	1600	0.102	0.001	11.02	0.0011	0	3.63×10^{-7}	9.1×10^{-4}	9.1×10^{-4}	N.D.	15.67
29–2	180	1600	0.104	0.01	11.21	0.00200	0	3.0×10^{-6}	0	2.0×10^{-6}	N.D.	14.74
29–3	166	1600	0.118	0.01	11.16	0.00199	0	2.1×10^{-6}	7.0×10^{-4}	7.0×10^{-4}	N.D.	14.84
22–1	58	1600	0.420	0.01	9.45	$<10^{-4}$	0	1.40×10^{-6}	0	1.93×10^{-6}	N.D.	14.47
22–2	76	1600	0.215	0.01	8.65	$<10^{-4}$	0	3.10×10^{-6}	0	2.84×10^{-6}	N.D.	14.42
22–3	80	1600	0.212	0.01	8.89	$<10^{-4}$	0	2.28×10^{-6}	2.1×10^{-4}	2.13×10^{-4}	N.D.	14.55
22–4	72	1600	0.206	0.01	8.69	$<10^{-4}$	0	2.02×10^{-6}	5.0×10^{-4}	5.00×10^{-4}	N.D.	14.62
22–5	122	1600	0.137	0.01	8.74	$<10^{-4}$	0	2.10×10^{-6}	7.5×10^{-4}	7.52×10^{-4}	N.D.	14.78

by these authors were not determined at steady-state conditions as evidenced by non stoichiometric Mg release relative to Si. This is discussed in detail below.

The initial stage of forsterite dissolution is always nonstoichiometric with preferential Mg release at pH $\leq$ 8 (Fig. 5a) but preferential Si release at pH $\geq$ 10 (Fig. 5b). Only slight preferential release of Fe over Mg has been detected for forsterite reacted in acidic solution (not shown) which is in agreement with faster dissolution rate of fayalite over forsterite (Wogelius and Walther, 1992). Stoichiometric Mg/Si release, however, is attained after a few hours and about 1 week in acidic and alkaline solutions, respectively. The rates depicted in Figure 4 are generated from Mg outlet concentration, but the error bars for each data point at pH $>$ 8 correspond to the difference R_{Si}–R_{Mg}. As seen in Figure 4, the rates decrease with a slope close to 0.5 at $1 \leq$ pH ≤ 9 and become nearly pH-independent (slope is $\sim$0.1) within the reproducibility of experiments at pH $\geq$ 9.5. Note that unlike forsterite dissolution rates reported by Blum and Lasaga (1988) and Wogelius and Walther (1991), the rates determined in this study do not

Table 2. Summary of Fo_{91} dissolution experiments performed at 25°C in CO_2-rich solutions. The units of R are mol/cm^2/s. Background electrolyte is NaCl/$NaHCO_3$/Na_2CO_3. N.D. = non determined. * = Experiments were performed at pCO_2 = 0.5 atm.

Exp #	Duration hrs.	Surface area, cm^2	Flow rate, mL/min	Ionic strength, M	pH	[Alk], M	$[Mg^{2+}]$, M input	$[Mg^{2+}]$, M output	[ΣSi], M input	[ΣSi], M output	$-\log R_{Si}$	$-\log R_{Mg}$
26–1*	43	3200	0.375	0.012	5.40	N.D.	0	5.10×10^{-5}	0	2.53×10^{-5}	13.31	13.26
26–2*	45	3200	0.652	0.012	5.44	N.D.	0	2.10×10^{-5}	0	9.92×10^{-6}	13.47	13.40
26–3*	30	3200	1.13	0.012	5.47	N.D.	0	1.16×10^{-5}	0	4.62×10^{-6}	13.57	13.42
26–4*	16	3200	2.48	0.012	5.44	N.D.	0	5.29×10^{-6}	0	2.62×10^{-6}	13.47	13.42
9–2	138	800	0.192	0.1	8.38	0.01	0	3.15×10^{-6}	0	1.65×10^{-6}	14.18	14.17
9–3	264	800	0.0768	0.1	8.55	0.01	0	4.23×10^{-6}	0	2.40×10^{-6}	14.42	14.43
9–4	111	800	0.198	0.1	8.50	0.01	0	2.06×10^{-6}	0	1.12×10^{-6}	14.33	14.33
9–5	96	800	0.384	0.1	8.53	0.01	0	1.49×10^{-6}	0	8.5×10^{-7}	14.17	14.18
2–3	178	1600	0.198	0.02	10.39	0.0162	0	8.0×10^{-7}	0	N.D.	N.D.	15.04
10–1	440	800	0.039	0.1	8.68	0.02	0	8.50×10^{-6}	0	4.25×10^{-6}	14.46	14.41
10–2	90	800	0.194	0.1	8.55	0.02	0	1.76×10^{-5}	0	1.0×10^{-6}	14.40	14.40
10–3	200	800	0.0965	0.1	8.63	0.02	0	3.03×10^{-6}	0	1.8×10^{-6}	14.44	14.47
16–1	52	800	0.502	0.1	8.46	0.05	0	3.0×10^{-7}	0	N.D.	N.D.	14.75
16–2	69	800	0.247	0.1	8.65	0.05	0	7.0×10^{-7}	0	N.D.	N.D.	14.70
16–3	164	800	0.126	0.1	8.71	0.05	0	1.20×10^{-6}	0	1.0×10^{-6}	14.60	14.76
16–4	288	800	0.0762	0.1	8.92	0.05	0	1.75×10^{-6}	0	1.0×10^{-6}	14.80	14.81
16–5	240	800	0.152	0.1	8.80	0.05	0	7.0×10^{-7}	0	3.0×10^{-7}	15.02	14.91
3–2	170	1600	0.203	0.1	11.15	0.04	0	1.05×10^{-6}	0	1.3×10^{-6}	14.57	15.10
3–3	144	1600	0.098	0.1	11.11	0.04	0	1.05×10^{-6}	0	2.7×10^{-6}	14.56	15.27
3–4	120	1600	0.196	0.1	11.10	0.04	0	7.3×10^{-7}	0	1.1×10^{-6}	14.65	15.13
3–5	57	1600	0.486	0.1	11.12	0.04	0	3.5×10^{-7}	0	6.0×10^{-7}	14.52	15.01
17–1	52	800	0.480	0.1	11.23	0.066	3.5×10^{-7}	4.4×10^{-7}	0	1.7×10^{-6}	N.D.	15.35
17–2	69	800	0.236	0.1	11.25	0.066	3.5×10^{-7}	5.36×10^{-7}	0	3.0×10^{-6}	N.D.	15.34
17–3	164	800	0.123	0.1	11.22	0.066	3.5×10^{-7}	5.5×10^{-7}	0	5.5×10^{-6}	N.D.	15.59
17–4	290	800	0.0617	0.1	11.22	0.066	3.5×10^{-7}	6.75×10^{-7}	0	9.4×10^{-6}	N.D.	15.68
17–5	240	800	0.123	0.1	11.23	0.066	3.5×10^{-7}	5.0×10^{-7}	0	9.0×10^{-6}	N.D.	15.72

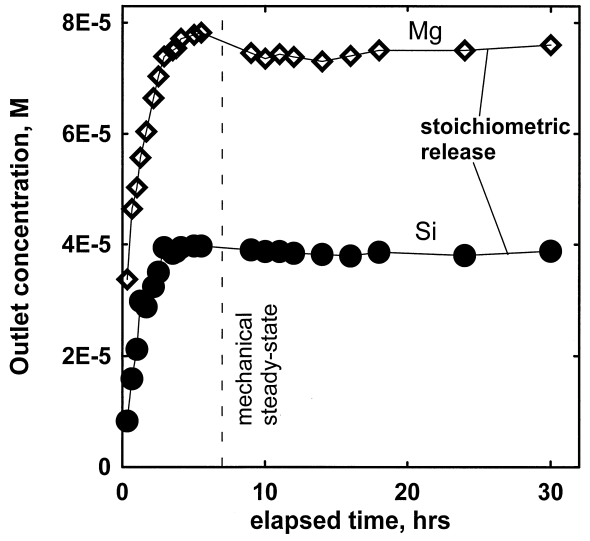

Fig. 2. Temporal evolution of the reactive fluid Mg and Si concentration during experiment No. 24-1 (pH = 3.0, I = 0.1 M NaCl)

exhibit a minimum at near neutral pH conditions. The solution ionic strength (I) seems to have a measurable effect on the dissolution rate at $3 \leq pH \leq 5$; a two-fold rate increase is observed when I increases from 10^{-3} to 10^{-1} M. Addition of Mg (up to 0.045 M) has no significant effect on the dissolution rate at pH 3 and 6.7 at constant ionic strength of 0.1 M as illustrated in Figure 6. This is in agreement with recent results of Oelkers (2000) and Rosso and Rimstidt (2000). In contrast, addition of Si leads to a significant decrease of the dissolution rate at pH ~ 9 and 11 (Fig. 7). The effect of carbonate ions on the forsterite dissolution rate at different pH is reported in Table 2 and Figure 8. The log R decreases linearly with log aCO_3^{2-} with a slope close to 1 at $aCO_3^{2-} > 10^{-4}$ M.

3.2. Forsterite Dissolution Mechanism

3.2.1. Acidic solutions

It has been shown in Part I of this study (Pokrovsky and Schott, 2000) that a silica-rich layer several unit cells thick forms on the forsterite surfaces in acidic to weakly alkaline solutions by the exchange of 2 hydrogen ions for a Mg atom. It was proposed that this reaction leads to the polymerization of isolated silica tetrahedra and allows the protons to penetrate/adsorb further on the surface. It was postulated, in agreement with the stoichiometry of forsterite titration, that the H^+ - Mg^{2+} exchange is followed by the adsorption of 0.5 H^+ per 1 forsterite surface site. Otherwise, the H^+ - Mg^{2+} exchange is followed by the adsorption of 1 proton on two polymerized silica tetrahedra. According to this scheme, the rate controlling surface complex can be formed by the following overall reactions:

$$>Mg_2SiO_4(surface) + 4H^+(aq) = >4H\text{-}SiO_4(surface) + 2Mg^{2+}(aq) \quad (1a)$$

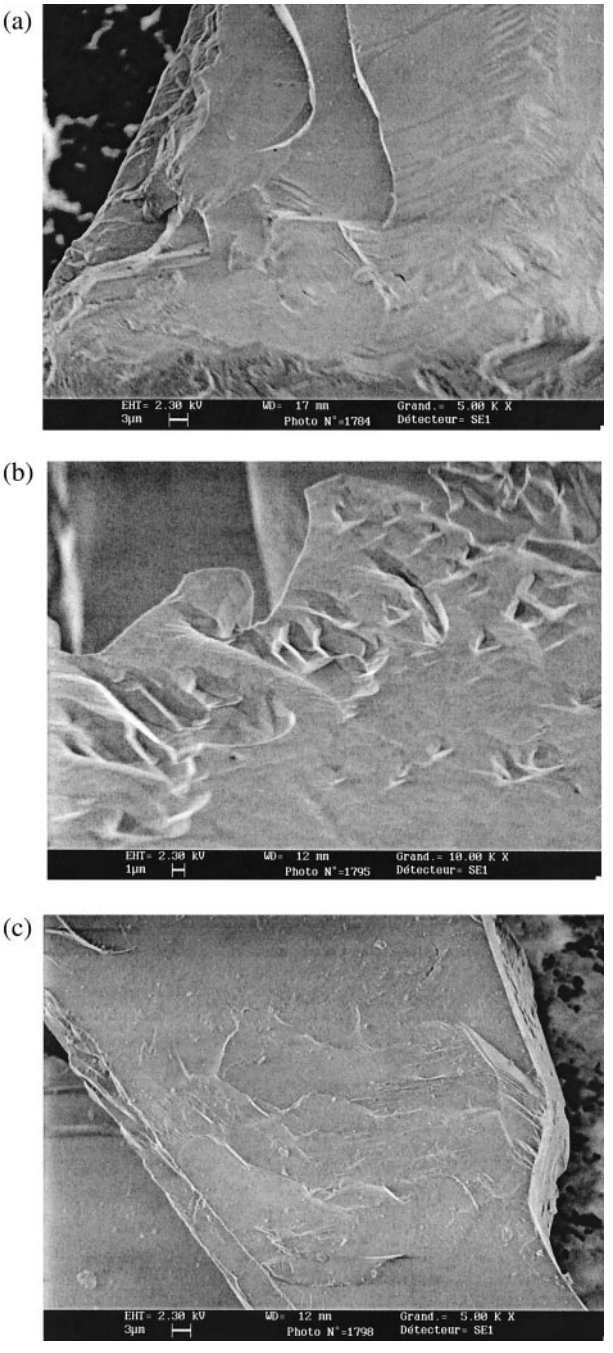

Fig. 3. SEM photomicrographs showing the surface of forsterite used in this study: (a) before dissolution experiments, (b) after experiment at pH 2, (c) after experiment at pH 11. Note the formation of etch pits in acid solutions (3b) and the absence of any secondary precipitation in alkaline solutions (3c). As compared to initial unreacted surface (Fig. 3a) there are always some very small adhering particles that disappear in acid solutions due to fast dissolution rate but persist in basic solutions.

$$K_{ex} = \frac{\{>4H - SiO_4\} \cdot a^2_{Mg^{2+}}}{a^4_{H^+} \cdot \{>Mg_2SiO_4\}} \quad (1b)$$

$$>4H\text{-}SiO_4(surface) + nH^+(aq) = >(4 + n)H\text{-}SiO_4(surface) \quad (2a)$$

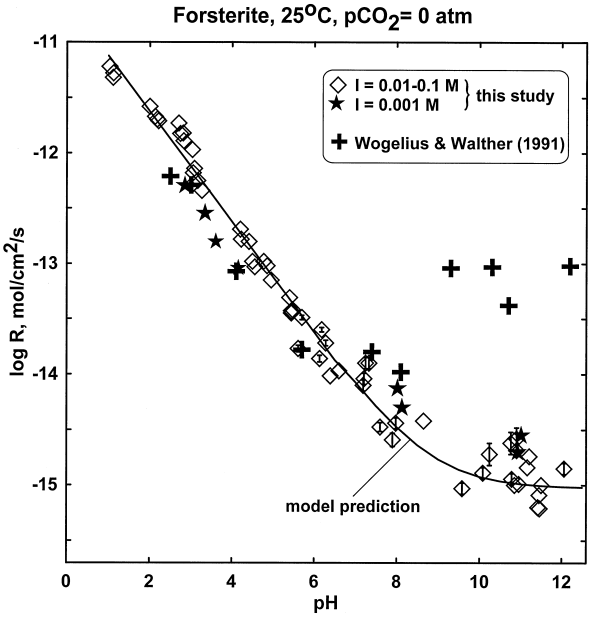

Fig. 4. Summary of forsterite steady-state dissolution rates at 25°C as a function of pH in CO_2-free solutions. The solid line represents a fit of experimental data to Eqn.15 (see explanation in the text). The crosses represent the results of Wogelius and Walther (1991); in their experiments, ionic strength was not fixed and adjusted by addition of HCl/NaOH.

$$K^*_{ads} = \frac{\{>(4+n)H - SiO_4\}}{a^n_{H^+} \cdot \{>4H - SiO_4\}} \qquad (2b)$$

where $\{>i\}$ is the concentration of surface species, a_i is the activity of aqueous species, and $n = 0.5$ (Pokrovsky and Schott, 2000). In Eqns. 1 and 2, K_{ex} and K^*_{ads} are the apparent stability constants of the exchange and adsorption reactions, respectively. These constants are conventional in the way that they are valid only at constant ionic strength of 0.1 M and the electrostatic term for surface reactions is equal to zero.

Mechanistically, omitting for simplicity the shared oxygen atoms in the polymerized layer, the polymerization of two silica surface sites followed by adsorption of one proton on the bridging oxygen of this dimer (overall reaction 2a) can be represented as:

$$> \text{SiOH} + \text{OHSi} < \rightarrow > \text{Si-O-Si} < + \text{H}_2\text{O} \qquad (3a)$$

$$> \text{Si-O-Si} < + \text{H}^+ \rightarrow > \text{Si-OH}^+\text{-Si} < \qquad (3b)$$

The forsterite surface shows an unreconstructed termination of the bulk structure with the measured cell dimensions on the surface similar to those of the bulk as confirmed by low energy electron diffraction (LEED) technique (Hochella, 1990). The outermost {010} surface consists of undercoordinated Mg atoms within a loosely packed sheet of oxygens, with Si and O in the next layer down (Hochella, 1990). In the forsterite structure, the closest distance between two Si tetrahedra is 3.65 Å which is comparable with Si-O-Si distance in non-protonated Si_2O_7 or fully protonated $H_6Si_2O_7$ dimers: 3.28 and 3.59 Å, respectively (Lasaga, 1995; Gibbs et al, 1994). Thus, the polymerization of at least each two isolated Si tetrahedra on the surfaces is possible provided that Mg octahedra are removed via an exchange reaction with H^+. Further polymerization requires participation of adsorbed water molecules, like in amorphous silica, in order to bring together the more distant Si tetrahedra (4.75 Å). Therefore, the surface layer of reacted forsterite can be seen as polymerized Si dimers connected with each other by common hydrogen-bonded water molecules and linked to the Mg octahedra deeper in the structure (Fig. 9a). Adsorption of proton occurs on bridging oxygens connected to Mg atoms deeper in the structure. Within this conceptual framework, the forward rate of overall dissolution reaction is controlled by decomposition of this protonated Si dimer and is given by:

$$R_{Si} \sim k_{Si} \cdot \{>Si_2O\text{-}H^+\} \qquad (4)$$

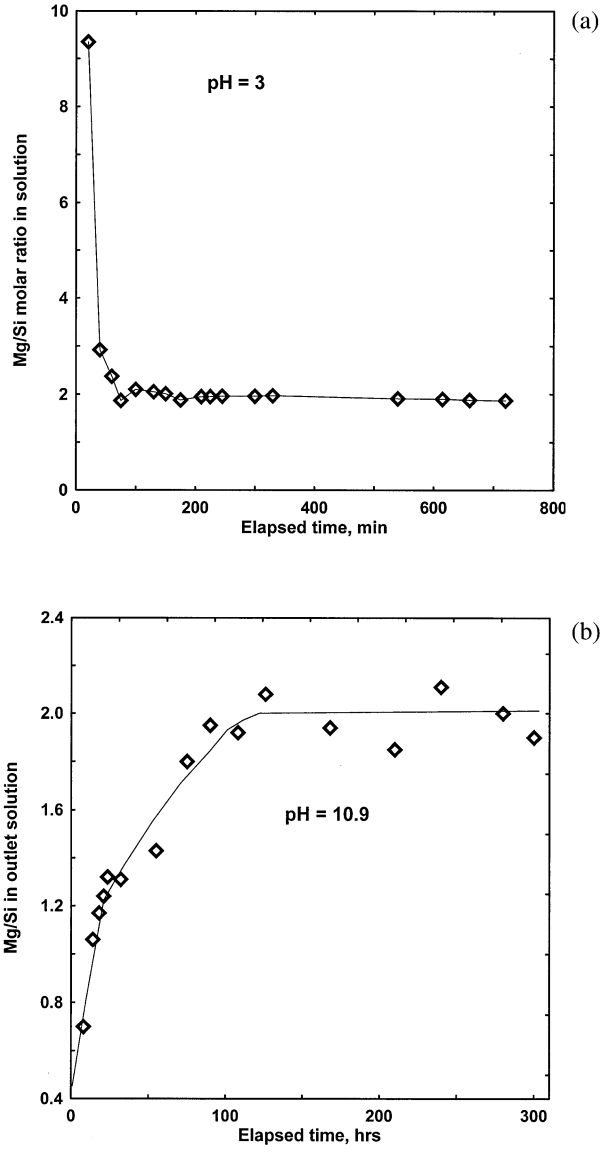

Fig. 5. The initial stage of forsterite dissolution: Mg/Si ratio in outlet fluid as a function of reaction time at pH 3 (a) and pH 10.9 (b). Preferential Mg release in acid solutions is consistent with formation of a Si-rich altered layer due to an exchange reaction with H^+. In alkaline solutions, preferential Si release indicates the formation of a Mg-rich layer on the surface.

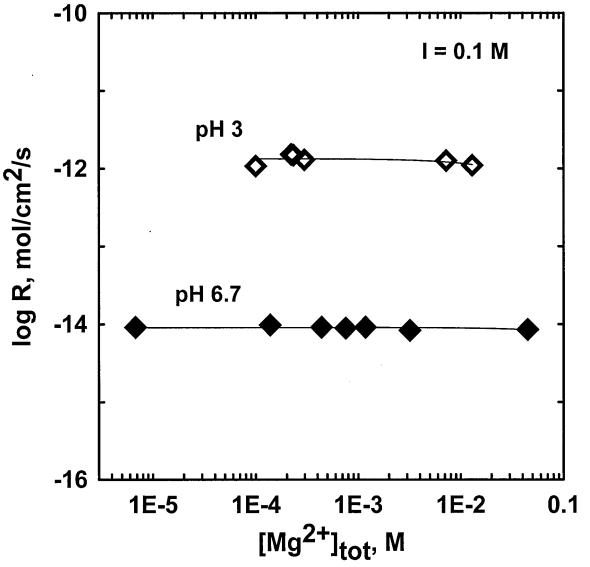

Fig. 6. Forsterite steady-state dissolution rate at 25°C as a function of aqueous Mg concentration in reactive fluid for pH 3 and 6.7. The lack of Mg influence on the forsterite dissolution rates is consistent with $K_{ex} > 10^{22}$ for reaction (1).

Assuming that the exchange and adsorption reactions occur on the surface sites initially occupied by magnesium, conservation of these sites yields

$$\{>Mg_2SiO_4\} + \{4H\text{-}SiO_4\} + \{(4+n)H\text{-}SiO_4\} = C = 2.2 \cdot 10^{-5}\ \text{mol/m}^2 \quad (5)$$

Combination of Eqns. 1b–2b and 4–5 using the assumption that the activities of the surface sites are equal to their concentrations gives

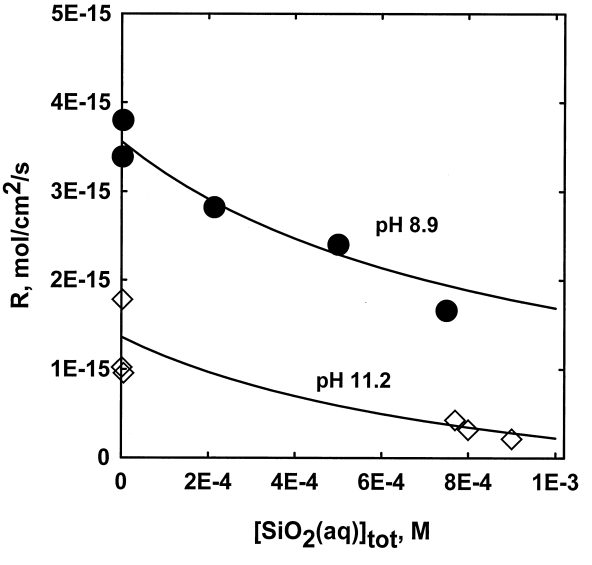

Fig. 7. Forsterite steady-state dissolution rate at 25°C as a function of silica concentration at pH 9 and 11. Data are from exp. No. 19–22. The solid lines represent a fit of experimental data to Eqns. 10 and 11 assuming $K^*_{Si} = 9 \cdot 10^{-4}$ (Eqn. 8) as described in the text.

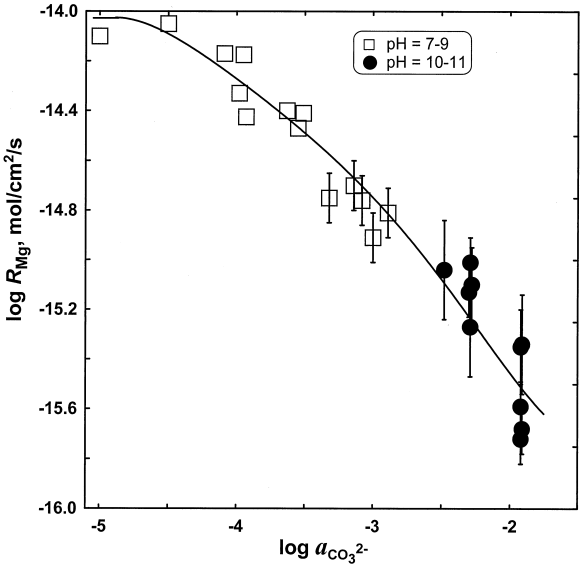

Fig. 8. Forsterite steady-state dissolution rates at 25°C as a function of CO_3^{2-} activity in solution. The rates are based on Mg release from the solid. The solid line represents a fit of experimental data to Eqn. 15 assuming $K^*_{Mg\text{-}CO3} = 10^{2.7}$ (Eqn. 14) as described in the text. Note that all solutions are undersaturated with respect to $MgCO_3$ (saturation index is below 0.1).

$$\{>Si_2O - H^+\} = 2.2 \cdot 10^{-5} \cdot \frac{K^*_{ads} \cdot a^{0.5}_{H^+}}{\left(1 + K^*_{ads} \cdot a^{0.5}_{H^+} + \frac{a^2_{Mg^{2+}}}{K_{ex} \cdot a^4_{H^+}}\right)} \quad (6)$$

where K_{ex} and K^*_{ads} are the equilibrium constants of reactions 1 and 2, respectively. Equation 6 can be further combined with Eqn. 4 to yield the following expression for forsterite dissolution rate

$$R_{Si} = k_{Si} \cdot \frac{K^*_{ads} \cdot a^{0.5}_{H^+}}{\left(1 + K^*_{ads} \cdot a^{0.5}_{H^+} + \frac{a^2_{Mg^{2+}}}{K_{ex} \cdot a^4_{H^+}}\right)} \quad (7)$$

The degree to which Eqn. 7 can be used to describe the forsterite dissolution rate at pH < 8 can be assessed in Figure 4 where the curve represents a fit of experimental data to Eqn. 7 assuming $k_{Si} = 2.38 \times 10^{-11}$ mol/cm^2/s, $\log K_{ex} \geq 22$, and $\log K^*_{ads} \leq 0.3$. The close correspondence between experimental data and the curve confirms that Eqn. 7 yields an excellent description of these data at pH < 8. Equation 7 is similar to that used by Brantley and Stillings (1996) to describe the dependence of feldspar dissolution rate on the surface concentration of protonated exchanged sites. Note, however, that unlike Na^+ and Al^{3+} for albite, Mg^{2+} does not inhibit forsterite dissolution because the Mg-H exchange reaction is very fast and $K_{ex} \geq 10^{22}$. Equation 7 should apply to any type of silicate whose dissolution is promoted by an ion-exchange reaction followed by the rate-controlling proton adsorption on exchanged sites.

3.2.2. Alkaline solutions

In alkaline solutions, preferential Si removal from forsterite surfaces leads to the formation of a Mg-rich layer as shown by

our XPS data and column filtration experiments (Pokrovsky and Schott, 2000). This suggests that, as in the case of other Mg-bearing minerals such as chrysotile (Bales and Morgan, 1985), magnesite (Pokrovsky and Schott, 1999), and dolomite (Pokrovsky et al., 1999), the hydrous cleavage of Mg-O bonds via hydrolysis of Mg surface sites should control forsterite dissolution. Note that the importance of surface hydration on forsterite dissolution rate at alkaline conditions was first recognized by Eriksson (1982).

Preferential Si release from forsterite surface in alkaline solutions is consistent with its surface structure: isolated SiO_4 tetrahedra can be easily removed from the surface leaving Mg octahedra branched together via Mg-O-Mg bonds like in brucite or Mg-bearing sheet silicates. A schematic polyhedral diagram of forsterite dissolution at these conditions is shown in Figure 9b.

The formation of the Mg-rich layer on forsterite surface ($>Mg_2SiO_4$) can be described by

$$>Mg_2SiO_4(\text{surface}) + 4H_2O = >Mg_2(OH)_4^{\circ}(\text{surface}) + H_4SiO_4(aq) \quad K_{Si}^* \quad (8)$$

Metal site conservation requires

$$X_{>Mg_2SiO_4} + X_{>Mg_2(OH)_4^0} = 1 \quad (9)$$

where X_i denotes the mole fraction of the ith surface species. Thus, the total concentration of Mg sites on this altered Si-deficient layer is given by

$$X_{>Mg_2(OH)_4^0} = K_{Si}^*/(K_{Si}^* + [SiO_2(aq)]_{tot}) \quad (10)$$

where K_{Si}^* is the equilibrium constant of reaction 8. The dissolution of this layer (Eqn. 11) requires the breaking of Mg-O-Mg bonds which is promoted by hydration of the forsterite surface with formation of $>MgOH_2^+$ species as it is the case for oxides (Stumm, 1992) or carbonates (Pokrovsky and Schott, 1999).

$$R_{Mg} = k_{Mg}\{>MgOH_2^+\} \quad (11)$$

These species are formed as a result of acid-base dissociation of neutral Mg centers exposed on the surface:

$$>MgOH^{\circ} + H^+ = >MgOH_2^+ \quad K_{int(12)} \quad (12)$$

$$>MgO^- + H^+ = >MgOH^{\circ} \quad K_{int(13)} \quad (13)$$

Their concentration can be calculated within the surface speciation approach by using a constant capacitance model with a double layer capacitance of 0.1 F/m^2. The conservation of magnesium surface sites implies

$$X_{>MgO^-} + X_{>MgOH^0} + X_{>MgOH_2^+} = X_{>Mg_2(OH)_4^0} \quad (14)$$

where $X_{>Mg_2(OH)_4}{}^0$ is the total concentration of Mg surface sites calculated from Eqn. 10. Due to the large number of parameters used in this modeling (concentrations of 3 surface species, and total amount of Mg and Si surface centers), it was not possible to derive an analytical expression for $\{>MgOH_2^+\}$. For each solution composition, $\{>MgOH_2^+\}$ was calculated using the MINTEQA2 code (Allison et al., 1991) and Eqn. 10. The initial values of surface intrinsic stability constants for reactions (12) ($K_{int(12)}$) and (13) ($K_{int(13)}$) were set to the corresponding values for MgO (Sverjensky and Sahai, 1996) which are also close to those for similar reactions in homogeneous solution as expected from the analogy between surface and solution chemical equilibria (Schindler and Stumm, 1987). Then, the dependence of experimental dissolution rates on pH was fitted using a different set of surface stability constants (12 and 13) by means of the MINTEQA2 code and Eqns. 10, 11, and 14. The sensitivity analysis performed to elucidate the relative role of different species demonstrated that at pH below 12, the contribution of $>MgO^-$ is not significant, thus only fitting of $K_{int(12)}$ was required. As a result, the following values of parameters in Eqns. 10–13 were derived: $k_{Mg} = 1.62 \times 10^{-10}$ mol/cm^2/s; log $K_{int(12)} = 11.5 \pm 0.5$ and log $K_{int(13)} = 12 \pm 2$. The scatter in experimental data did not allow determination of the values of intrinsic stability constants with an uncertainty lower than ± 0.5 log units.

The inhibition of forsterite dissolution by dissolved silica in basic solutions is illustrated in Figure 7 where the solid lines represent a fit of experimental data to Eqn. 10 and 11 with $K_{Si}{}^* = (9 \pm 1) \times 10^{-4}$. Increase of pCO_2 to 0.5 atm at pH of 5.4 does not have any influence on forsterite dissolution rates as measured in this study (Exp. No. 26 of Table 2).

Taking into account these results, the following general rate equation can be proposed to describe forward forsterite dissolution at all pH conditions

$$R_T = R_{Si} + R_{Mg} = k_{Si} \cdot \frac{K_{ads} \cdot a_{H^+}^{0.5}}{\left(1 + K_{ad} \cdot a_{H^+}^{0.5} + \frac{a_{Mg^{2+}}^2}{K_{ex} \cdot a_{H^+}^4}\right)} + k_{Mg}\{>MgOH_2^+\} \quad (15)$$

This equation accounts for two parallel reactions occurring at silica-rich and hydrated Mg sites, respectively. The degree to which Eqn. 15 can be used for describing Fo dissolution rate in carbonate-free solutions may be assessed in Figure 4, where the solid line depicts the rate computed with Eqn. 15. Bearing in mind the high uncertainties of dissolution rate determinations at pH above 9, the close correspondence between the curve and the bulk of the experimental data demonstrates their consistency with Eqn. 15 and supports the hypothesis that forsterite dissolution is controlled by two parallel reactions occurring at Si-rich and Mg-rich sites in acid and alkaline solutions, respectively. To illustrate the composition of possible surface precursor complexes involved in the reaction control, a schematic two-dimensional diagram of forsterite surface in acid and alkaline solutions is presented in Figure 9c.

The control of forsterite dissolution by the hydrolysis of Mg surface groups at pH > 9 also accounts for its inhibition by dissolved carbonate via the formation of $>MgCO_3^-$ surface species:

$$>MgOH_2^+ + CO_3^{2-} = >MgCO_3^- + H_2O, K_{Mg\text{-}CO3}^* \quad (16)$$

The solid line in Figure 8, where the dissolution rates in carbonate-bearing solutions are presented, was calculated using Eqn. (15) with log $K_{Mg\text{-}CO3}^* = 2.7$. This value is similar to that of $MgCO_3^o$ (aq) ion pair formation in homogeneous solutions reflecting again the analogy between aqueous and surface equilibrium. Note that a similar mechanism for inhibiting forsterite dissolution by dissolved CO_2 was suggested by Wogelius and

Fig. 9. Schematic diagrams depicting the surface structure of forsterite in acidic (a) and alkaline (b) conditions, and precursor complexes (c) that control forsterite dissolution. Tri-dimensional olivine structures were created using Crystal Impact software (DIAMOND—Visual Crystal Structure Information System; CRYSTAL IMPACT, POSTFACH 1251, D-53002 Bonn) 9a. The surface layer of acid-reacted forsterite is seen as polymerized Si dimers connected with each other by common hydrogen-bonded water molecules and linked to the Mg octahedra deeper in the structure. Protons adsorb/penetrate on Si-O-Si bridging oxygens thus forming a surface complex controlling the overall dissolution rate. 9b. Preferential release of isolated SiO_4 tetrahedra from the forsterite surface in alkaline solutions leads to formation of residual Mg octahedra like in brucite. Hydrous cleavage of Mg-O-Mg bonds via formation of $>MgOH_2^+$ surface precursor complexes should be a rate-controlling step for these conditions.

Walther (1991) but with the adsorption of one aqueous carbonate ion on two magnesium surface centers.

3.3. Comparison with Previous Results

3.3.1. Acidic solutions

Forsterite dissolution rates obtained at pH below 8 in this study are in fair agreement with most available data. The reaction order with respect to H^+ of about 0.5 is close to the value reported by Luce et al. (1972); Blum and Lasaga (1988), Wogelius and Walther (1991), and Rosso and Rimstidt (2000). However, there are some discrepancies concerning the reaction mechanism for forsterite dissolution in acid solutions. The rate limiting step proposed in this study, decomposition of protonated polymerized silica tetrahedra linked to Mg atoms deeper in the structure, combines the ion-exchange mechanism suggested by Blum and Lasaga (1988) with proton adsorption on metal-oxygen (Murphy and Helgeson, 1987; Oelkers, 1999; Oelkers, 2000) or bridging Si-O-Mg bonds (Rosso and Rimstidt, 2000). This dissolution mechanism is close to that proposed by Stillings and Brantley (1996) for feldspar dissolution, i.e. rate controlling proton adsorption on exchanged surface sites. This reflects the similarity in formation of surface precursor complexes for all silicate minerals in acidic solutions. The relative importance of ion-exchange versus proton surface adsorption reactions is determined by the thermodynamic values K_{ex} and K_{ads} for the corresponding reactions, i.e., the relative strength of the metal-oxygen bonds that have to be broken before the rate-limiting hydrolysis of Si-O bonds.

3.3.2. Basic solutions

Only Blum and Lasaga (1988) and Wogelius and Walther (1991) investigated forsterite dissolution rates in alkaline solutions (pH $>$ 8). The most striking difference between the results of this study and those of Blum and Lasaga (1988) and Wogelius and Walther (1991) is that an increase of the dissolution rate with pH at pH $>$ 8 in CO_2-free solution is not observed in the present work (Fig. 4). There is no clear explanation of these differences. However, it should be noted that the primary data of Blum and Lasaga (1988) and Wogelius and Walther (1991) do not unequivocally support their claim of an increase of forsterite dissolution rate in alkaline solutions. Unlike this study, none of their experiments reached stoichiometric dissolution (i.e., steady state). As a result, their rate values, calculated on the basis of "initial" Si release, may be overestimated compared to rates determined at steady-state/stoichiometric dissolution. As was shown in the first part of this study (Pokrovsky and Schott, 2000) and in Figure 5b of the present work, there is always preferential Si release from fresh Fo surfaces at pH $\geq$ 10 with silica concentrations up to 100 times higher than those of Mg. Note also that the number of data points collected in previous studies at alkaline conditions was not enough to minimize the effect of random errors in calculated rates: Blum and Lasaga (1988) report only one rate value at pH $\sim$ 11 and Wogelius and Walther (1991) collected four values in the alkaline region which show that Mg-based dissolution rates actually do not depend on pH for 9 $\leq$ pH $\leq$ 12 (see Fig. 4). It is important to note, however, that the data collected by Wogelius and Walther (1991) in solutions open to the atmosphere at pH $>$ 8 show a plateau of pH-independent dissolution rates at $R \sim 10^{-14.4}$ mol/cm^2/s which is in quite reasonable agreement with the results of this study. Both studies thus yield comparable forsterite weathering rates in surficial aquatic environments open to atmospheric CO_2.

For other silicate minerals, only a few studies addressed the effect of CO_2 on mineral dissolution rates. According to Knauss et al. (1993), the removal of dissolved CO_2 via nitrogen bubbling through solution does not appear to have any significant effect on diopside dissolution rates at 8 $\leq$ pH $\leq$ 12. Brady and Carroll (1994) did not find any effect of pCO_2 ($10^{-3.5}$ to 1 atm) on augite and anorthite dissolution at pH 4, whereas Berg and Banwart (2000) reported very strong increase of anorthite dissolution rates in the presence of CO_3^{2-}. Unfortunately, in the latter study, only non-stoichiometric dissolution was reported, which does not allow evaluation of the mechanism of reaction. Brady and Gíslason (1997) found no effect of pCO_2 ($10^{-3.5}$ to $10^{-2.3}$ atm) on the basalt glass dissolution rates at pH 8. In contrast, Xie (1994) observed a very strong inhibiting effect of atmospheric CO_2 on wollastonite dissolution rate at 10 $\leq$ pH $\leq$ 12. Generally, the effect of CO_2 for most silicate minerals is very weak in acid to neutral solutions but may be important in alkaline conditions.

The mechanism of forsterite dissolution in basic solutions proposed in this study, implies that the rate controlling step is the detachment of hydrolyzed surface magnesium ions. This is consistent with the observation of Westrich et al. (1993) that the dissolution rates of various end-member orthosilicates correlate with the rate for water exchange from the solvent into the hydration sphere of the corresponding cation. Thus, the hydrolysis of Me-O bonds seems to be the critical step for all orthosilicate minerals dissolution in alkaline solutions. This is also supported by the inhibiting effect of CO_3^{2-} which may occur only by adsorption of carbonate ions on $>MgOH_2^+$ groups as proposed by Wogelius and Walther (1991) and in this study. Such a mechanism is contradictory to that proposed by Brady and Walther (1989) who postulated that the rupture of

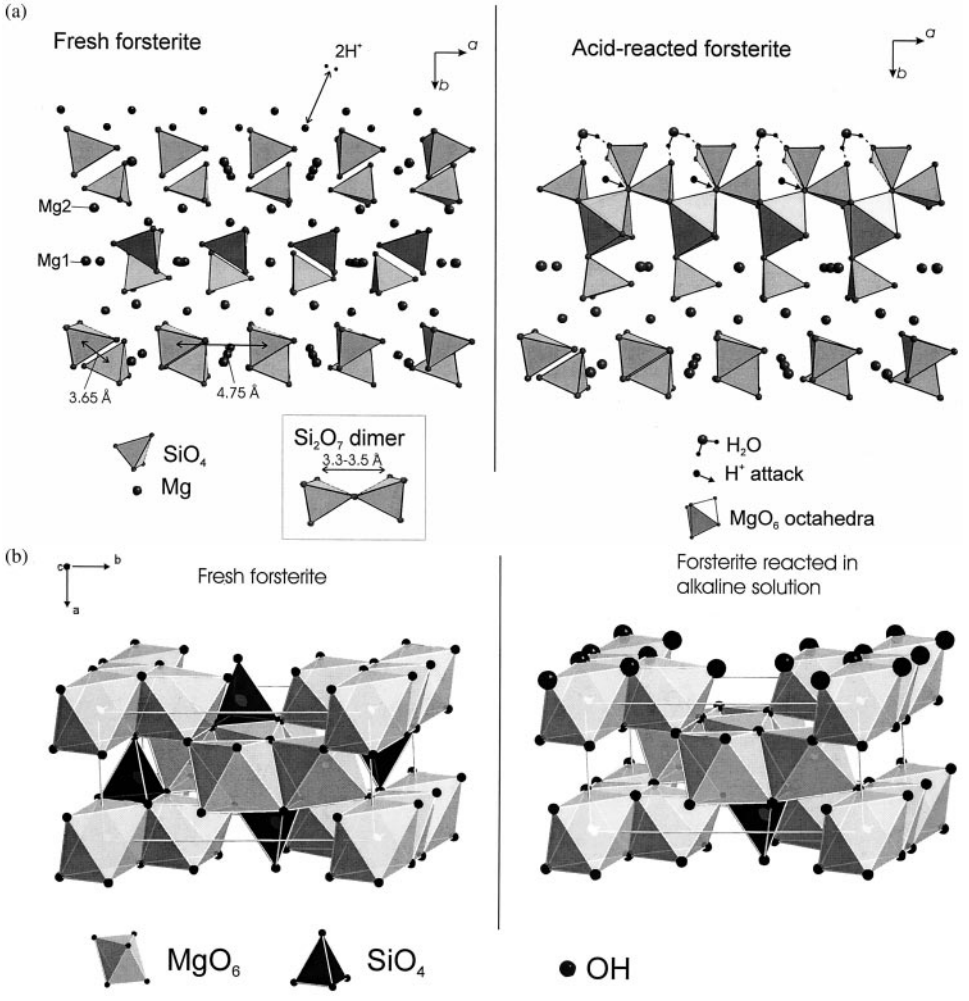
(a)
Fresh forsterite
2H+
a
b
Mg2
Mg1
3.65 Å
4.75 Å
SiO4
Mg
Si2O7 dimer
3.3-3.5 Å
Acid-reacted forsterite
H2O
H+ attack
MgO6 octahedra
(b)
c
b
a
Fresh forsterite
Forsterite reacted in alkaline solution
MgO6
SiO4
OH

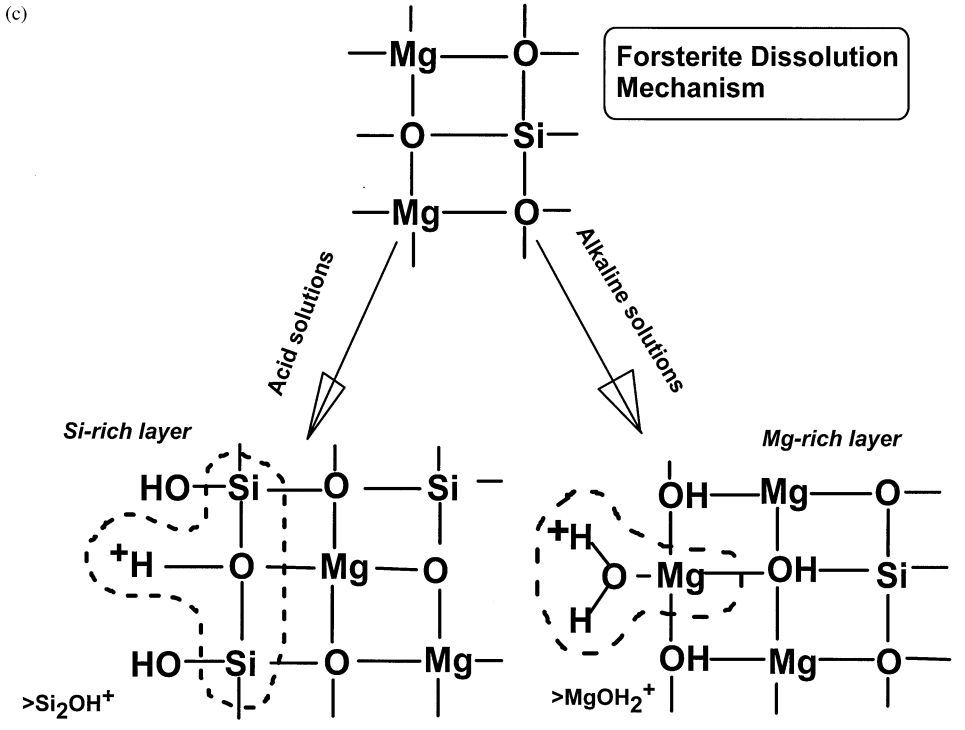
(c)
Mg
O
Si
Forsterite Dissolution Mechanism
Acid solutions
Alkaline solutions
Si-rich layer
Mg-rich layer
HO
Si
H
OH
>Si2OH+
>MgOH2+

Si-O bonds via the deprotonation and hydrolysis of $>SiOH^o$ surface species is the rate-controlling step for all silicate dissolution at alkaline conditions. Obviously, for orthosilicates, unlike for feldspars and sheet silicates, breaking of Si-O bonds in alkaline solutions is not necessary to dismantle the mineral structure which is comprised of isolated SiO_4 tetrahedra crosslinked by chains of edge-sharing octahedra occupied by divalent metals.

4. APPLICATIONS

Based on the results obtained in this study and available literature information, one may estimate the effect of CO_2 on the dissolution rates of orthosilicates at neutral to alkaline pH conditions. Unlike at pH below 9, dissolution of forsterite in alkaline solutions is strongly inhibited by aqueous carbonate ions. This effect becomes significant at ΣCO_2 values as low as 10^{-3} M which are often met in the course of basalt or ultramafic rock weathering in natural surficial environments. At pH 10, for example, in a solution in equilibrium with atmospheric CO_2, $aCO_3^{2-} = 10^{-1.66}$ and $\Sigma CO_2 = 0.14$ M (!). Springs from partially serpentinized peridotites and dunites or fresh ultramafic rocks contain up to 0.024 M ΣCO_2 at pHs close to 9 (Barnes and O'Neil, 1969). Gíslason and Arnórsson (1993) measured pHs of 8.5 to 10 in surficial waters in contact with basaltic rocks. Moreover, pH values of 11 to 12 have been frequently reported for ground waters in contact with ultramafic rocks throughout the world (Nesbitt and Bricker, 1978). At these conditions, dissolved carbonate in equilibrium with atmospheric CO_2 significantly affects forsterite dissolution rates that can be up to 1 order of magnitude lower than those computed without taking account of CO_3^{2-} inhibition. It is worth noting that a similar aqueous carbonate effect was also reported for wollastonite by Xie (1994). This author observed a 2 and 2.5 orders of magnitude decrease of wollastonite dissolution rate in the presence of atmospheric CO_2 in solutions at pH of 10 and 12, respectively. Increase of atmospheric pCO_2 would increase ΣCO_2 in solutions whose pH is buffered at 10 ± 1 by basaltic and ultramafic rocks. The subsequent decrease of forsterite dissolution rate should result in a decrease of atmospheric CO_2 consumption, i.e., unlike for feldspars, there is a negative feedback between pCO_2 and forsterite weathering rate at alkaline conditions.

5. CONCLUDING REMARKS

Knowledge of forsterite surface chemistry obtained by various macroscopic and spectroscopic techniques has proved to be crucial for interpreting forsterite dissolution rate over a wide range of pH at 25°C. In acidic to weakly alkaline solutions, forsterite H^+-promoted dissolution is controlled by the decomposition of a silica-rich, Mg-free, protonated surface precursor complex formed by the fast exchange of $2H^+$ for one Mg^{2+} ion followed by sorption of one proton on two polymerized silica tetrahedra. This mechanism is consistent with the development of a hydrogen permeated leached layer where residual hydrated silicate tetrahedra are polymerized and probably linked to Mg ions deeper in the mineral structure.

At $pH > 9$, it is the hydration of surface Mg sites with the formation of $>MgOH_2^+$ species which controls dissolution. Preferential Si release, observed at the initial stage of dissolution, together with results of XPS analysis (Pokrovsky and Schott, 2000), is consistent with the formation of a Mg-rich layer on the surface. The breaking of Mg-O-Mg bonds in this altered surface layer is thus the critical step for forsterite dissolution at these conditions. Inhibition of dissolution rate by dissolved silica and CO_3^{2-} is assumed to stem from the formation of Si-deficient precursor complexes containing hydrated surface Mg groups, $>MgOH_2^+$. It is possible that a similar mechanism controls the dissolution of all divalent-metal bearing silicates in neutral to basic solutions. Inhibition of forsterite dissolution rate by dissolved CO_2 at alkaline conditions may have important consequences that cannot be ignored when modeling the chemical weathering of silicate minerals and its feedback on atmospheric CO_2. Unlike for the weathering of aluminosilicates, increase of atmospheric CO_2 leads to a decrease of ultramafic rock weathering rates in basic solutions. Further work is necessary to check if similar negative feedback occurs between pCO_2 and the weathering rates of other Mg and Ca silicates, the minerals that exert a major long term control on the atmospheric CO_2 budget.

Acknowledgments—We acknowledge the insightful and very constructive reviews of K. L. Nagy, D. Wesolowski, and two anonymous reviewers. The authors are grateful to M. Thibaut and M. Goujon for careful technical assistance with XRD and B.E.T. analyses, respectively. M. Okab is thanked for assistance with the SEM analysis. E. Oelkers and R. Wogelius are thanked for the useful discussions. This work was supported by a visiting research position awarded to O. P. by CNRS.

Editorial handling: D. J. Wesolowski

REFERENCES

Allison J. D., Brown D. S., and Novo-Gradac K. J. (1991) MINTEAQA2/PRODEFA2, A geochemical assessment model for environmental systems: Version 3.0 user's manual. U.S. EPA, Athens, GA.

Awad A., Van Groos A. F. K., Guggenheim S. (2000) Forsteritic olivine: Effect of crystallographic direction on dissolution kinetics. *Geochim. Cosmochim. Acta* **64,** 4765–4772.

Bales R. and Morgan J. J. (1985) Dissolution kinetics of chrysotile at pH 7 to 10. *Geochim. Cosmochim. Acta* **49,** 2281–2290.

Barnes I. and O'Neil J. R. (1969) The relationship between fluids in some fresh alpine-type ultramafics and possible modern serpentinization, Western United States. *Geol. Soc. Amer. Bull.* **80,** 1947–1960.

Berg A. and Banwart S. A. (2000) Carbon dioxide mediated dissolution of Ca-feldspar: Implications for silicate weathering. *Chem. Geol.* **163,** 25–42.

Blum A. and Lasaga A. (1988) Role of surface speciation in the low-temperature dissolution of minerals. *Nature* **331,** 431–433.

Brady P. V. and Carroll S. A. (1994) Direct effects of CO_2 and temperature on silicate weathering: Possible implications for climate control. *Geochim. Cosmochim. Acta* **58,** 1853–1856.

Brady P. V. and Gíslason S. R. (1997) Seafloor weathering controls on atmospheric CO_2 and global climate. *Geochim. Cosmochim. Acta* **61,** 965–973.

Brady P. V. and Walther J. V. (1989) Controls on silicate dissolution rates in neutral and basic pH solutions at 25°C. *Geochim. Cosmochim. Acta* **53,** 2823–2830.

Brantley S. L. and Stillings L. (1996) Feldspar dissolution at 25°C and low pH. *Am. J. Sci.* **296,** 101–127.

Casey W. H., Westrich H. R., Banfield J. F., Ferruzi G., and Arnold G. W. (1993) Leaching and reconstruction at the surfaces of dissolving chain-silicate minerals. *Nature* **366,** 253–256.

Chen Y. and Brantley S. L. (2000) Forsterite dissolution at 65°C and $2 < pH < 5$. *Chem. Geol.* **165,** 267–281.

Eriksson E. (1982) On the dissolution rate of forsterite in aqueous solutions. *Vatten* **38,** 409–415.

Gibbs G. V., Downs J. W., Boisen M. B., Jr. (1994) The elusive SiO bond. In *Silica, Physical Behavior, Geochemistry, and Material Applications* (eds. P. J. Heaney, C. T. Prewitt, and G. V. Gibbs); *Rev. Mineral.* **29,** 331–368.

Gíslason S. R. and Arnórsson S. (1993) Dissolution of primary basaltic minerals in natural waters: Saturation state and kinetics. *Chem. Geol.* **105,** 117–135.

Grandstaff D. E. (1978) Changes in surface area and morphology and the mechanism of forsterite dissolution. *Geochim. Cosmochim. Acta* **42,** 1899–1901.

Grandstaff D. E. (1986). The dissolution rate of forsteritic olivine from Hawaiia beach sand. In *Rates of Chemical Weathering of Rocks and Minerals* (eds. S. M. Colman and D. P. Dethier); Academic Press.

Hochella M. F., Jr. (1990) Atomic structure, microtopography, composition, and reactivity of mineral surfaces. In *Mineral-Water Interface Geochemistry* (ed. M. F. Hochella, Jr. and A. F. White); *Rev. Mineral.* **23,** 87–132.

Knauss K. G., Nguyen S. N., and Weed H. C. (1993) Diopside dissolution kinetics as a function of pH, CO_2, temperature, and time. *Geochim. Cosmochim. Acta* **57,** 285–294.

Lasaga A. C. (1995) Fundamental approaches in describing mineral dissolution and precipitation rates. In *Chemical Weathering Rates of Silicate Minerals* (eds. A. F. White and S. L. Brantley); *Rev. Mineral.* **31,** 23–86.

Luce R. W., Bartlett R. W., and Parks G. A. (1972) Dissolution kinetics of magnesium silicates. *Geochim. Cosmochim. Acta* **36,** 35–50.

Murphy W. M. and Helgeson H. C. (1987) Thermodynamic and kinetic constraints on reaction rates among minerals and aqueous solutions: III. Activated complex and the pH-dependence of the rates of feldspar, pyroxene, wollastonite, and forsterite hydrolysis. *Geochim. Cosmochim. Acta* **51,** 3137–3153.

Nesbitt H. W. and Bricker O. P. (1978) Low temperature alteration processes affecting ultramafic bodies. *Geochim. Cosmochim. Acta* **42,** 403–409.

Oelkers E. H. (1999) A comparison of enstatite and forsterite dissolution rates and mechanisms. In *Growth and Dissolution in Geosystems* (eds. B. Jamveit and P. Meakin) pp. 253–257, Kluwer.

Oelkers E. H. (2000) An experimental study of forsterite dissolution kinetics as a function of temperature and aqueous Mg and Si concentration. *Chem. Geol.*, in revision.

Pokrovsky O. S. and Schott J. (1999) Processes at the magnesium-bearing carbonates/solution interface. II. Kinetics and mechanism of magnesite dissolution. *Geochim. Cosmochim. Acta* **63,** 881–897.

Pokrovsky O. S., Schott J., and Thomas F. (1999) Dolomite surface speciation and reactivity in aquatic systems. *Geochim. Cosmochim. Acta* **63,** 3133–3143.

Pokrovsky O. S. and Schott S. (2000) Forsterite surface composition in aqueous solutions: A combined potentiometric, electrokinetic, and spectroscopic approach. *Geochim. Cosmochim. Acta,* **64,** 3299–3312.

Rosso J. J. and Rimstidt J. D. (2000) A high resolution study of forsterite dissolution rates. *Geochim. Cosmochim. Acta* **64,** 797–811.

Sanemasa I., Yoshida M., and Ozawa T. (1972) The dissolution of forsterite in aqueous solutions of inorganic acids. *Bull. Chem. Soc. Japan* **45,** 1741–1746.

Schindler P. W. and Stumm W. (1987) The surface chemistry of oxides, hydroxides, and oxide minerals. In *Aquatic Surface Chemistry* (ed. W. Stumm), 337–365. Wiley.

Schott J. and Berner R. A. (1983) X-ray photoelectron studies of the mechanism of iron silicate dissolution during weathering. *Geochim. Cosmochim. Acta* **47,** 2233–2240.

Schott J. and Berner R. A. (1985) Dissolution mechanisms of pyroxenes and olivines during weathering. In *The Chemistry of Weathering* (ed. J. J. Drever) pp. 35–53. D. Riedel Publ. Co.

Siegel D. I. and Pfannkuch H. O. (1984) Silicate mineral dissolution at pH 4 and near standard temperature and pressure. *Geochim. Cosmochim. Acta* **48,** 197–201.

Siever R. and Woodford N. (1979) Dissolution kinetics and the weathering of mafic minerals. *Geochim. Cosmochim. Acta* **43,** 717–724.

Stumm W. (1992) Chemistry of the Solid-Water Interface. Wiley.

Sverdrup H. (1990) The Kinetics of Base Cation Release due to Chemical Weathering. Lund University Press.

Sverdrup H. and Bjerle I. (1982) Dissolution of calcite and other related minerals in aqueous solutions in a pH-stat. *Vatten* **38,** 59–73.

Sverjensky D. A. and Sahai N. (1996) Theoretical prediction of single-site surface-protonation equilibrium constants for oxides and silicates in water. *Geochim. Cosmochim. Acta* **60,** 3773–3797.

Westrich H. R., Cygan R. T., Casey W. H., Zemitis C., and Arnold G. W. (1993) The dissolution kinetics of mixed-cation orthosilicate minerals. *Am. J. Sci.* **293,** 869–893.

Wogelius R. A. and Walther J. V. (1991) Forsterite dissolution at 25°C: Effects of pH, CO_2, and organic acids. *Geochim. Cosmochim. Acta* **55,** 943–954.

Wogelius R. A. and Walther J. V. (1992) Forsterite dissolution kinetics at near-surface conditions. *Chem. Geol.* **97,** 101–112.

Xie Z. (1994) Surface properties of silicates, their solubility and dissolution kinetics. Ph. D. thesis, Northwestern Univ.